THE JOURNAL OF PHYSICAL CHEMISTRY B

Article

pubs.acs.org/JPCB

Hofmeister Effects in Monoclonal Antibody Solution Interactions

Dejan Arzenšek,*[,†,‡,¶] Drago Kuzman,[†] and Rudolf Podgornik[¶,§]

[†]Sandoz Biopharmaceuticals Mengeš, Lek Pharmaceuticals d.d., Kolodvorska 27, Mengeš SI-1234, Slovenia

[‡]Netica storitve d.o.o., Reteče 97, Škofja Loka SI-4220, Slovenia

[¶]Department of Physics, Faculty of Mathematics and Physics, University of Ljubljana, Jadranska 19, Ljubljana SI-1000, Slovenia

[§]Department of Theoretical Physics, J. Stefan Institute, Jamova cesta 39, Ljubljana SI-1000, Slovenia

ABSTRACT: By using static and dynamic light scattering (SLS and DLS), we investigate the effect of ion specificity and solution conditions on the solution behavior of monoclonal antibodies (mAbs). The extracted second virial coefficient, a global measure of the strength of protein−protein interactions, shows a complicated, nonmonotonic behavior. It can be connected on one side with the Hofmeister effect, and on the other with the interplay of screening and charge fluctuations in inhomogeneous, patchy charge distribution of these particular proteins. Although direct quantification in terms of the underlying long and short-range potentials is out of reach, the observed effects do point toward important features of mAbs solution aggregation processes that are governed by the identity of the solution ions as well as by details of the charge distribution of interacting proteins.

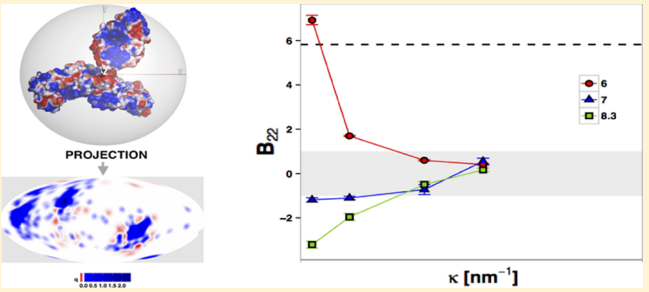

INTRODUCTION

Aggregation and stability of globular proteins in general, and of therapeutic monoclonal antibodies in particular, is determined by the long- and short-range interactions mediated by the electrolyte solution environment.[1] The phenomenology of these nanoscale interactions[2] and its theoretical framework within the Deryaguin−Landau−Verwey−Overbeek (DLVO) theory of colloid stability[3,4] provide a useful conceptual landscape in order to understand the intricacies of (bio)-physicochemical interactions[5] that connect the structure with the activity of various biologically relevant macromolecules. Nevertheless, as reiterated recently by Prausnitz,[6] despite its usefulness, the assumptions inherent in the DLVO framework of protein−protein interactions do have serious limitations.

Currently, therapeutic monoclonal antibodies (mAbs) have emerged as a part of a rapidly growing class of pharmaceutical products and a powerful method for treating many terminal diseases because they are effective at low concentrations with fewer side effects compared to other small molecule drugs.[7] The quest for designing promising lead molecules and subsequently stable formulations at high concentrations poses challenges related to the propensity of proteins to aggregate at the higher concentrations. These challenges have stimulated interest in understanding the physicochemical aspects as well as the solution behavior of mAbs which are critical for development of more stable therapeutic drugs.[8] Understanding the detailed nature of the protein−protein interactions between mAbs at various solution conditions[7] has consequently gained momentum.[9−11] Understanding the solution-mediated interactions between mAbs would elucidate its complex aggregation phase behavior and possibly enable the selection of optimized solution properties in the therapeutic context.[12]

Although the final goal of these studies on protein−protein interactions would be the full separation and orientation dependent intermolecular potential, the available experimental techniques do not yet allow for this kind of detailed resolution. In fact, a direct experimental assessment of the strength and separation dependence of protein−protein interactions in solution by, for example, the osmotic stress method, the surface force apparatus or AFM experiments[13] is currently not (yet) possible. The only readily available quantitative but indirect measure of protein−protein interactions in aqueous solutions is B_{22}, their *second virial coefficient* in dilute solution conditions.[14] The second virial coefficient quantifies the deviations of a protein solution from ideality, in the sense that $B_{22} > 0$ indicates predominant net mutual repulsive interaction, while $B_{22} < 0$ indicates a predominant net protein−protein attraction, the connection being rather *indirect* since the second virial coefficient is a global property of the interactions, proportional to an integral of the interaction potential over all separations and orientations.[15] Combining the static and dynamic light scattering (SLS and DLS) determination of B_{22} with a plausible DLVO framework provides us then with qualitative and sometimes quantitative means to understand some salient features of the protein−protein interactions.[16]

While the equilibrium part of the colloidal interactions is dominated by the two main types of long-range interactions

Received: March 13, 2015
Revised: July 20, 2015

DOI: 10.1021/acs.jpcb.5b02459
J. Phys. Chem. B XXXX, XXX, XXX−XXX

between proteins, that is, the van der Waals[17] and the electrostatic[13] interactions, constituting the well-known attractive-repulsive DLVO dichotomy,[3,4] they can be sometimes crucially modified by the presence of explicit non-DLVO interactions such as hydration, hydrophobic, and steric interactions.[18] The electrostatic part of the DLVO theory is based on the Poisson−Boltzmann (PB) electrostatics, which predicts screened repulsion between like-charged colloidal spheres in an electrolyte solution at moderate salt concentrations. Furthermore, the electrostatic interaction itself can contain a substantial infusion of the nonelectrostatic effects, as exemplified by the notion of the *Hofmeister series*, originally observed in the context of protein solution precipitation for various salts in terms of a universal series of ionic activity.[19] Protein aggregation, crystallization, precipitation, gelation, or liquid−liquid phase separation[20−22] all show substantial Hofmeister effects. Although various attempts to rationalize the Hofmeister series have been made,[23] the only valid consensus seems to be the uncontested role of nonelectrostatic interactions in determining the ionic specificity.[24,25] Because protein solution precipitation is connected with the protein−protein interaction potential, the Hofmeister effects should certainly be detectable in the virial coefficient behavior and could be possibly exploited in order to control the stability of protein solutions.[26] A number of experimental studies of mAb thermodynamic behavior have focused upon the analysis of the most important features of protein−protein interactions, such as protein charge distribution and effective molecular size, analyzing protein solution behavior as a function of solution pH, ionic strength,[12,27−34] identity of added salts and/or buffers,[26,35−37] as well as effects of specific amino acid sequence motifs[38,39] in conjunction with computational studies.[40−42] In particular, the work of Roberts et al. has shed important light on the intricacies of the electrostatic component to the protein−protein interactions between monoclonal antibodies,[10,26] which are related to the salt-specificity effects,[43] buffer composition, and the charge distribution anisotropy.[44] The anisotropy in protein−protein interactions can have different origins, stemming either from patchy interaction sites with angularly dependent interaction potentials,[45] anisotropic charge distribution,[15,46,47] or from protein shape anisotropies.[48,49] All these effects are mutually connected and difficult to disentangle. In order to separate the complicated topology of the protein surface from the inhomogeneous charge distribution, it is appropriate to introduce global-to-local representation models of molecular surfaces at various levels of sophistication.[50]

To address the specific ion-effects in solution properties of the IgG1 monoclonal antibody (mAb) and to investigate its interactions in aqueous ionic solutions, we investigate the second virial coefficient with SLS and the interaction parameter by DLS, under differing pH conditions and in the presence of different types of salts chosen in such a way that they fit into widely different Hofmeister series positions. The goal of this study is thus 2-fold: to measure the second virial coefficient for this protein and to assess the ion-specific effects in its behavior. In order to accomplish this program, we used NaCl, NaSCN, and Na_2SO_4 salts at pH = 6.0, 7.0, and 8.3 and salt concentrations between 60 and 600 mM, performing a full salt concentration and pH scan for each salt type, complementing in this way a different set of experiments by Roberts et al.[26] The complicated behavior of the second virial coefficient and the underlying protein−protein interaction points to effects of possibly widely different origin, such as ion specificity, charge distribution, and screening, and although it is difficult to disentangle the ion-specific effects from the charge anisotropy, that on its own depends on the dissociation equilibrium of the protein surface, we will interpret the second virial coefficient data in terms of the net-charge of the protein, possible effects of protein charge anisotropy, ionic screening, and fluctuations in the ionic atmosphere.

MATERIALS AND METHODS

Materials and Sample Preparation. The model IgG1 monoclonal antibody (mAb), with molecular weight of 145 × 10^3g/mol and pI of 8.46 measured by isoelectric focusing (IEF), was obtained from Sandoz Biopharmaceuticals Mengeš as stock solution of 50 mg/mL in histidine hydrochloride buffer at pH 6.0 and used without further purification. The sample purity (>99%) was confirmed by size exclusion chromatography. Solution properties of this molecule have been studied extensively in our previously published study.[9] The buffer and salt reagents were obtained from Merck Millipore (Merck KGaA, Darmstadt, Germany) and Sigma-Aldrich Chemical (St. Louis, MO, U.S.A.). All chemicals used were reagent grade unless specified. Deionized Milli-Q grade water was used to prepare all solutions. Buffer sodium phosphate was prepared to maintain the solution pH in pH range of 6.0, 7.0, and 8.3. Appropriate buffer concentrations were selected via Henderson−Hasselbalch equation to maintain the low total ionic strength at 20 mM without the addition of salt. All buffer solutions were then passed through 0.22 μm PVDF Millipore filters (Billerica, MA, U.S.A.). The purified stock mAb formulation was concentrated to approximately 220 mg/mL using an Amicon 8050 stirred ultrafiltration cell with ultrafiltration membranes of 30K MWCO (Merck-Millipore, Germany) and then placed in a Slide-A-Lyser dialysis cassette with a maximum volume of 30 mL and a 10K MWCO (Thermo Scientific Ltd., U.K.). Approximately 30 mL stock solutions were dialyzed against 2 L buffer for each pH over 48 h for a minimum of 3 times at 5° C. The dialyzed sample and the dialyzate were filtered against 0.22 μm PVDF filters and then stored at ∼5° C and used for further use. Final mAb stock concentrations of 205 mg/mL (pH 6.0) and 175 mg/mL (pH 7.0 and 8.3) were determined by using gravimetric dilutions and an UV absorptivity at 280 nm (A280) using extinction coefficient of α_{280} = 1.48 $(mg/mL)^{-1}$ cm^{-1} for 0.1% (w/v) protein solutions. The extinction coefficient was determined by quantitative amino acid analysis. For higher ionic strengths, the stock solutions (1.2M) of NaCl, NaSCN, and Na_2SO_4 salts were added to the mAb stock solution to get the target final salt concentrations of I = 60, 300, and 600 mM. All the experiments were performed in the concentration series in different concentration ranges. mAb stock solutions for corresponding concentration range were prepared by gravimetric dilution and subsequent filtration using a 0.02 μm syringe filter (when viscosity was too high at a higher stock concentration, 0.1 or 0.2 μm syringe filters were used). The same 0.02 μm syringe filter was used on the prepared buffers and salt stock solutions before being used in the measurement. The diluted mAb stock solutions were allowed to reach thermal and chemical equilibrium at controlled room temperature for at least several hours. Protein solutions were centrifuged at room temperature for at least 30 min at 3000 rpm to remove adventitious dust and bubbles from the bulk of the solutions used for light scattering analysis.

DOI: 10.1021/acs.jpcb.5b02459
J. Phys. Chem. B XXXX, XXX, XXX−XXX

Size-Exclusion Chromatography with Multi-Angle Light Scattering (SEC-MALS). The SEC-MALS experiments were conducted using a serially connected Agilent HPLC intrument with photodiode array detector (Agilent), G3000SWXL 7.8 mm × 300 mm size exclusion chromatography column (Tosoh Bioscience), a three-angle miniDAWN TREOS (Wyatt Technology) multiangle light-scattering (MALS) detector and Otpilab rEX (Wyatt Technology) differential refractive index (RI) detector. The mobile phase was composed of phosphate-buffered saline (PBS) buffer (GIBCO), and its flow rate was 0.7 mL/min. Column temperature was ambient and samples were held at 5° C prior to injection. Chromatographic and light scattering data were analyzed using ASTRA 6 software (Wyatt Technology) and Empower software (Waters).

To determine the overall fractional polydispersity of mAb monomers versus irreversible oligomers (formed by irreversible aggregation) or impurities (large aggregates) and to assess monomer molecular weight M_W by size exclusion separation, we used the SEC-MALS method for all three pH buffer conditions. The chromatography elution profiles indicate two fraction peaks with a homogeneous molecular weight of ∼147 × 10^3 g/mol for the main peak and ∼360 × 10^3 g/mol for the oligomeric peak. The same values were obtained for all pH conditions and for subsequent experiments with increased injected concentrations, for which the obtained molecular weights were constant across the peak and for each injection concentration.

For all cases studied, the attractive interactions measured by CG-MALS method appear to be too weak to impact the SEC-MALS data, because it is known[43] that strong attractions contribute to the heterogeneous molecular weight profile because of the aggregation. The molecular weight value of main peak agrees nicely with the calculated value from protein primary sequence data of 145.5 × 10^3 g/mol by taking into account the additional contribution of attached glycans of ∼1−3 × 10^3 g/mol. The oligomeric value overlaps with the value between a dimer and a trimer. By calculating the area of the main monomeric and oligomeric peaks relative to the total peak area, the fraction of monomers is determined to be ∼99% and oligomeric peak less than ∼1% (Table 1). Thus, the oligomer peak fraction does not impact the weight-averaged nominal molecular weight *bulk M*. To confirm this result, the *bulk* molecular weight was measured by CG-MALS measurements in fixed mAb concentration solution conditions in the absence of the SEC column dilution effects. This value corresponds closely to the M_W calculated across all these eluting peaks as analyzed in the Results section.

Table 1. Results of Calculated Fractions from the SEC Method for pH 6.0, 7.0, and 8.3 without Added Salt

pH	monomer fraction [%]	oligomer fraction [%]
6.0	99.8	0.2
7.0	99.1	0.4
8.3	98.6	0.9

Static Light Scattering. Static light scattering using multiangle scattering was performed to experimentally obtain the second virial coefficient B_{22}. In the static case, the excess Rayleigh scattered light intensity R_θ of a protein solution relates to the osmotic compressibility through the slope of the static scattering intensity data in a Debye plot in its reciprocal format as[9,10,51]

$$\frac{Kc}{R_\theta}\left(\frac{\partial n}{\partial c}\right)_A^2 = \frac{K^*c}{R_\theta} = \frac{1}{RT}\left(\frac{\partial \Pi}{\partial c}\right)_A \simeq \frac{1}{M} + 2B_{22}c \quad (1)$$

where A indicates fixed T, μ_1, μ_3 conditions. B_{22} being proportional to an integral over space, is a global characteristic of the interaction potential, at low protein concentration conditions. Here, c is the mass concentration of the proteins (in g/mL), M is their molecular weight, Π is the osmotic pressure, $\frac{\partial \Pi}{\partial c}$ is the osmotic compressibility, and T is the absolute temperature.

The above equation describes the system protein (index 2), water (index 1), and salt (index 3), therefore the partial derivatives are at constant temperature T, and chemical potentials of water μ_1 and salt μ_3. $R_\theta = R(q)$ is the excess Rayleigh ratio[51,52] that depends on the scattering angle θ through the wavenumber $q = \frac{4\pi n_0}{\lambda_0}\sin\left(\frac{\theta}{2}\right)$. Furthermore, $K^* = K\cdot(\partial n/\partial c)^2_{T,\mu_1,\mu_3} \simeq (2\pi n_0(\mathrm{d}n/\mathrm{d}c))^2/N_A\lambda_0^4$ is the system specific optical constant, λ_0 is the wavelength of laser incident light, n_0 the solvent refractive index, and $(\mathrm{d}n/\mathrm{d}c)$ the refractive index increment with protein concentration. R is the molar gas constant ($R = N_A k_B$) and N_A is the Avogadro number. The refractive index increment has been measured extensively for protein solutions and is equal to ≃0.185 mL/g.

For determination of the B_{22}, the samples are prepared at various protein concentrations under the same solution conditions. The measured K^*c/R_θ values are plotted as a function of concentration c, and a linear function is fitted using eq 1. The ordinate intercept (in the limit of infinite dilutions $c \to 0$) is equal to $1/M$ and B_{22} is determined from the slope of the line. The experimental figure of merit (FOM), defined as[53,54] FOM = $|2B_{22}Mc|$, is the minimum statistically significant fraction of scattered light from interaction contributions relative to the linear ideal scattering term. It determines the confidence of B_{22} when we assume the relative error of measured M_{app} as 5%.

R_θ is measured for a finite series of protein concentrations and then used, eq 1, to obtain fitted parameters. In order to assess the deviations from the linearity implied by eq 1, the experiments were performed across a wide range of protein concentrations (0.3−198 mg/mL). The Rayleigh scattering deviations from ideal solution behavior are obtained from the ratio R_θ/K^*.[53−55] Net average attractions (repulsions) are manifest as upward (downward) curvature in the linear concentration behavior of this ratio.

The universal nonspecific interaction quantified by B_{22} is the isotropic hard-sphere repulsion due to the protein excluded volume. It can be used to identify a minimum concentration at which protein solution displays nonideal thermodynamic behavior. It can also be used to assess the relative magnitude of soft attractive/repulsive contributions with respect to the underlying excluded volume contribution as the difference $B_{22}^{soft} = B_{22} - B_{22}^{HS}$.[10,15] A negative difference indicates a soft attractive, whereas a positive difference a soft repulsive interaction. B_{22}^{HS} can be calculated as[10,56]

$$B_{22}^{HS} = \frac{4v_{eff}^{HS}}{M},\quad v_{eff}^{HS} = \frac{4\pi N_A r_H^3}{3M} \quad (2)$$

DOI: 10.1021/acs.jpcb.5b02459
J. Phys. Chem. B XXXX, XXX, XXX−XXX

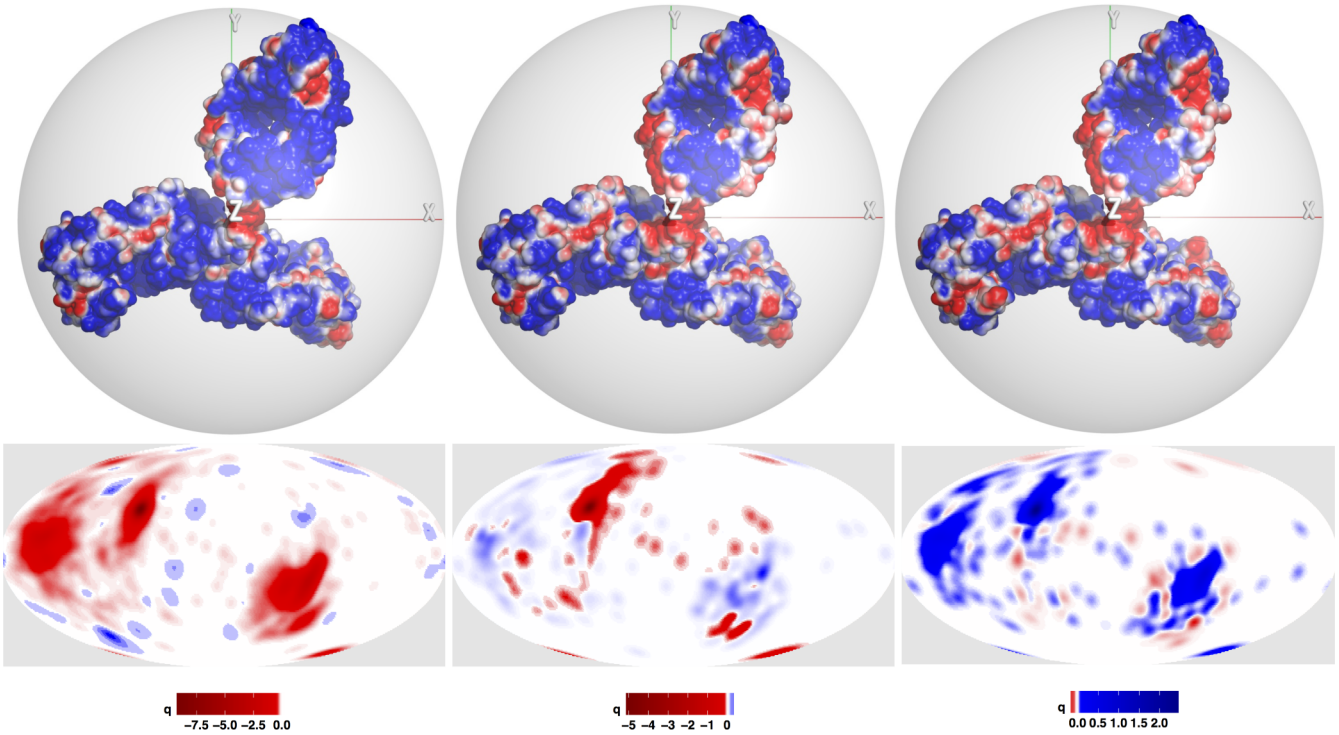

Figure 1. Top row: A visualization model for space charge distribution around the protein at pH = 6.0, 7.0, and 8.3. The space charge was mapped onto solvent-accessible surface (SAS) from the calculated electrostatic potential using the APBS solver. Negative (red) and positive space charge (blue) projected onto the SAS appear as charge patches trailing the SAS surface topology. We inscribe the whole protein inside a sphere centered on its center of mass. Bottom row: Calculated pH dependence of the IgG1 monoclonal antibody (mAb) fixed charge distribution at pH = 6.0, 7.0, and 8.3 projected onto a fictitious circumscribed spherical surface and visualized in the Mollweide projection. Monopolar as well as dipolar patches are clearly visible. The parameter W = 5 Å was used (see main text). Note that the upper figures represent the space charge around the protein, while the lower ones represent the fixed charge of the protein.

where the hard-sphere radius can be measured as the hydrodynamic radius r_H by DLS.[57] It overestimates the actual radius of the protein as it assumes an ideal spherical shape (see Figure 1). Here, v_{eff}^{HS} is the protein spherical effective volume, differing from the protein's actual partial specific volume v_{sp} (in the case investigated v_{sp} = 0.73 cm^3/g[9]) due to spherical shape approximation. The hydrodynamic radius was determined at 60 mM salt concentration for each solution pH from the value of $D_0 = 4.5 \pm 0.06 \times 10^{-7}$ cm^2/s, in the limit of infinite dilution as r_H = 5.4 nm. These values compare with our previous published work with $D_0 = 4.43 \times 10^{-7}$ cm^2/s[9] and fall into the previously published experimental range of $4.16–4.54 \times 10^{-7}$ cm^2/s.[28,34,38,58,59] On the basis of this estimate of r_H, we assume a constant protein radius a = 5 nm, regardless of protein concentration and/or solution conditions. For molecular weight M, the value of 147×10^3 g/mol obtained by SLS was used, which also agrees nicely with the molecular weight obtained by SEC-MALS. Using these values, we obtained the estimated value of $B_{22}^{HS} = 5.8 \times 10^{-5}$ mol·mL/g^2, which we used to estimate the minimum concentration of incipient nonideality as ≃4.3 mg/mL. We set the minimum statistically significant value as FOM = 0.05. For 0.05 < FOM < 0.2, the concentration dependence of the total light scattered is well described by a first-order fit in eq 1. The linear concentration range, suitable for B_{22} determination, was set with simultaneous estimation of B_{22} FOM value below 0.2 and negligible values for B_{222}.

From the assumed protein hard-sphere radius of 5 nm, we obtain v_{eff}^{HS} = 2.1 cm^3/g, corresponding to a specific volume in the absence of electrostatic repulsion (i.e., at pH 8.3 near the mAb's IEP). The difference w.r.t v_{sp} reflects the effect of bound water, which is also a lower bound to the excluded volume for any cosolute molecule that is larger than a water molecule.[60]

A three-angle miniDAWN TREOS (Wyatt Technology) multiangle light scattering (MALS) detector (100 mW GaAs diode laser with λ_0 = 658 nm) was used for all scattering measurements. Filtered HPLC grade toluene was used for calibration of the voltage and light scattering intensities. MALS detector was connected to the Calypso II (Wyatt Technology) automated syringe sample preparation and delivery system with three syringe pumps. Calypso delivered sample to the MALS detector, and then the sample is transferred to the Otpilab rEX (Wyatt Technology) differential refractive index (RI) detector with extended concentration range for inline concentration measurements. Technical description of connected instrumentation in the *s.c.* composition-gradient MALS (CG-MALS) method was described elsewhere,[10,61] but here the combined method was used with Claypso II where sample was delivered into the flow cell and manually mixed samples were measured in a microCuvette.

For the Calypso experiment, different mAb stock solutions were prepared by dilution with low enough concentrations and with the low enough sample viscosities, below ∼10 cP. For sample concentrations above this viscosity limit, the back-pressure on the syringe pumps is too high and the dilutions were made manually and samples were measured in a microCuvette. To prevent saturation of MALS detectors, the sensitivity was reduced according to the scattered light intensity. The CG-MALS approach allows us to measure samples with higher accuracy with reduced sample dilution and mixing errors in order to focus on the detailed effects of fine

DOI: 10.1021/acs.jpcb.5b02459
J. Phys. Chem. B XXXX, XXX, XXX−XXX

variations of pH as well as the ionic strength of the salt solutions for buffer conditions which were problematic to measure due to these measurement errors (e.g., pH near protein IEP).

Data were processed using Calypso software and obtained for all three angles assuming isotropic scattering. All three angle values were weighted equally and were averaged (linear extrapolation to zero angle with zero-angle order) to use in the following analysis. All three angle values are shown in the plots to clearly show the dispersion of experimental data.

Dynamic Light Scattering. To quantify the relation between pairwise protein interactions and protein diffusion in solution, the relation between B_{22} and the collective diffusion constant D_c was investigated using dynamic light scattering (DLS). In the hydrodynamic regime, diffusivities derived from DLS are ascribed to the collective diffusion constant D_c, which is controlled by a chemical potential gradient, viz., the drag force exerted on a particle from the solvent, and interparticle hydrodynamic and long-range interactions as mediated by the solvent. For small volume fractions, one can relate the collective diffusion constant to the solute properties as[9,10,62−64]

$$D_c = D_0(1 + k_D c) \tag{3}$$

Here, the interaction parameter k_D may be split into several different contributions and D_0 is the single particle diffusion coefficient related to the hydrodynamic particle radius r_H (assumed to coincide with the interaction radius) via the Stokes−Einstein relation $D_0 = k_B T/6\pi\,\eta\,r_H$, where η is the solvent viscosity. The hydrodynamic radius r_H is the radius of a sphere that has the same diffusion coefficient as the protein. The interaction parameter k_D reflects all the interactions between proteins, which control their collective motion. The correlation between k_D and B_{22} was analyzed recently, and it indicates that while k_D provides a measure of protein−protein interactions and is in fact connected with B_{22},[58,65] this connection hinges on additional assumptions that make it less straightforward than in the case of pure equilibrium experiments that give the B_{22} directly, without any further hypotheses.[9,10] The excluded volume hard-core contribution to the interaction parameter is given by the sum over all virial and hydrodynamic terms, expressible as[66]

$$k_D^{HC} = 0.39 B_{22}^{HS} M \tag{4}$$

Using the value $B_{22}^{HS} = 5.8 \times 10^{-5}$ mol·mL/g^2 and $M = 147 \times 10^3$ g/mol, we get $k_D^{HC} = 3.3$ mL/g.

DLS analysis was also used to observe concentration-dependent changes in mutual diffusion coefficient D_c. Oligomers with molecular weight in the order of dimers or trimers will cause an increase in overall average r_H and therefore the decrease of D_0, rather than a second distinct peak.

DLS linear concentration regime was determined by fitting eq 3 until the second-order interaction parameter has a negligible value in the same way as described for CG-MALS SLS. The DLS measurements were however performed at much lower concentrations than for SLS due to DLS instrument limitations at high concentrations. DLS data for pH 7.0 and 8.3 at 300 and 600 mM Na_2SO_4 were excluded from further consideration, becuse they did not pass the polydispersity index (PdI) limit of 0.1 for monodisperse peaks, where PdI is the square of the relative standard deviation, $\sigma_{D_c}^2 = (\langle D_c^2\rangle - \langle D_c\rangle^2)/\langle D_c\rangle^2$. The ordinate intercept (in the limit of infinite dilutions $c \to 0$) is equal to D_0 (used in the B_{22}^{HS} determination), and k_D is determined from the slope of the line.

DLS measurements were conducted using a Malvern Instruments Zetasizer APS (the temperature-controlled auto plate sampler) (Worcestershire, U.K.). Further details of the experimental methodology are given in previous publication.[9] For DLS, samples were collected after performing the SLS measurements using CG-MALS method. While SLS is a more sensitive probe of the pair molecular interaction than DLS, the latter provides additional information on particle sizes, as well as kinetic behavior inaccessible to SLS. The most important advantage of k_D is that it can be rapidly measured using a multiwell plate DLS plate reader with minimal sample consumption.

Surface Charge Distribution Mapping. In order to quantify the nonuniform charge distribution of the IgG1 monoclonal antibody, while including the possibility of changes in the charge state of the surface residues, we separate the effects of the anisotropy induced by the complicated shape of the protein from those due to the inhomogeneous charge distribution. We assume that the protein can be modeled with a circumscribed sphere with radius R but with an anisotropic surface-projected charge density. This global-to-local representation of molecular surfaces can be formulated on various levels of sophistication by deforming the original solvent accessible protein surface into an effective sphere.[50]

A three-dimensional IgG1 mAb representative computer model was constructed by modifying the X-ray crystallographic structure using Swiss-PdbViewer[67] to reconstruct the final IgG1 antibody PDB atomic structure data in the same manner as in our previous publication.[9] The atomic structure was furthermore based on an MD relaxation that presumably gives the most likely conformation of IgG1 in solution.[41,68] Atomic partial charges and all atomic radii were obtained from the PARSE force field topology file.[69,70] The full mAb structure was then used to obtain the pK_a values of individual charged residues by using PROPKA 3.0 software,[71,72] which were then used as an input for the PDB2PQR software tool,[73] the conventionally used software for calculating the electrostatic properties of proteins. The space charge distribution then depends on the complete distribution of ionizable amino acid residues in the protein structure, as well as on the pH of the solvent.[47,74] The electrostatic potential surface mapped on the mAbs solvent-accessible surface (SAS) was calculated using the Adaptive Poisson−Boltzmann Solver program (APBS),[75] implementing the linearized Poisson−Boltzmann (PB) equation. For dielectric constants, we used 2 inside the protein and 78 for the solvent. The ion concentration (0.02 M) and a cubic B-spline discretization was used for charge distribution. Finally, PyMol[76] was used to create 3D graphical representations of the mAb and its electrostatic potential isosurfaces, superimposed on the original SAS. From the electrostatic potential, the continuum space charge can be computed as an excess electrical charge on the superimposed SAS surface rather than as distinct point-like charges. The resulting space charge distribution is represented in Figure 1 (top row), where we can clearly see the differences for different pH values of 6.0, 7.0, and 8.3. From the visualization, it is clear that the obtained space charge distribution does not adequately reflect the fixed charge distribution and that direct visualization of the fixed charges would be preferable.

To circumvent this problem, we used another direct mapping of surface charges onto a circumscribed sphere for further 3D

DOI: 10.1021/acs.jpcb.5b02459
J. Phys. Chem. B XXXX, XXX, XXX−XXX

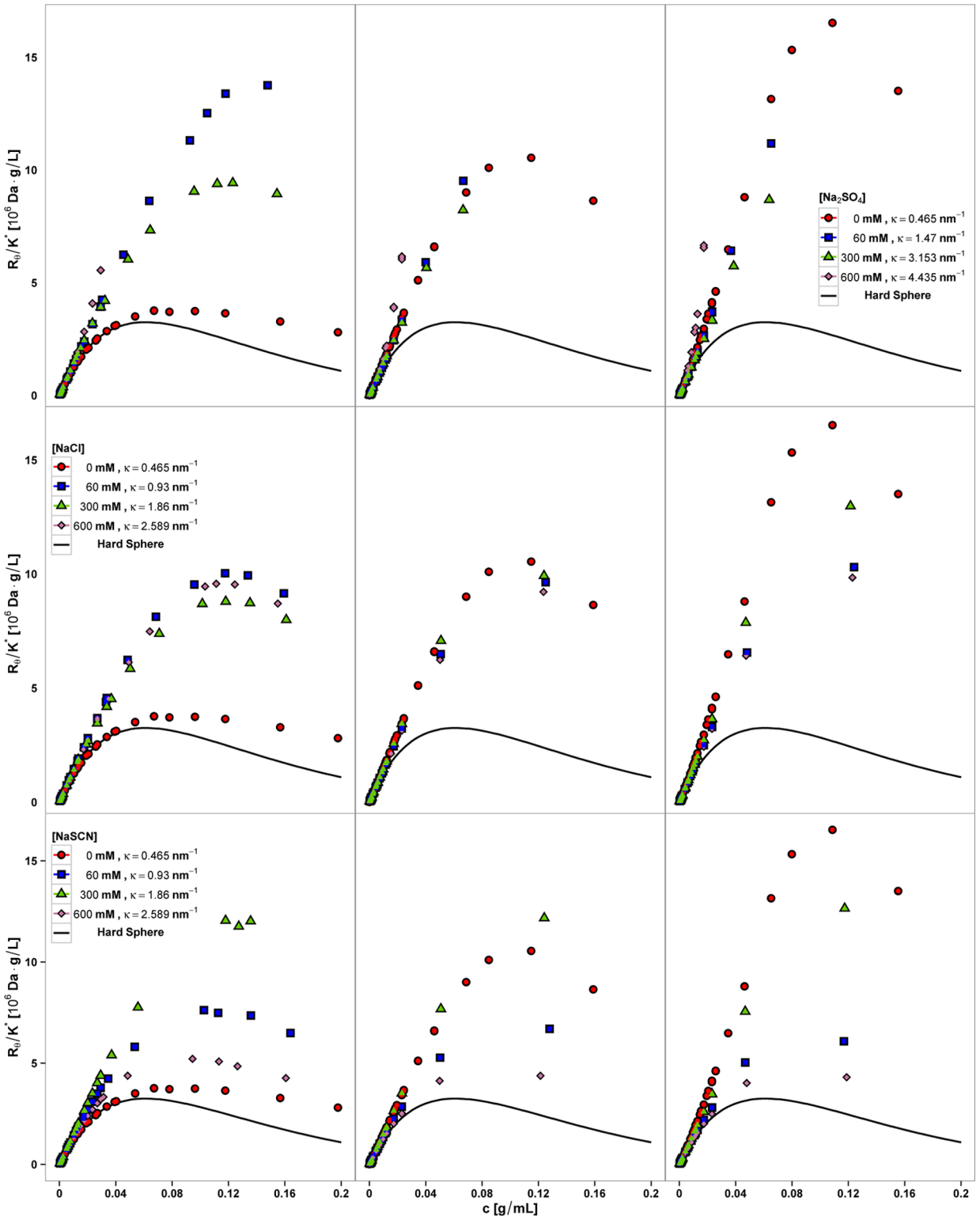

Figure 2. Concentration dependence of static light scattering intensity signal R_θ/K^* at pH = 6.0, 7.0, and 8.3 with varying Na_2SO_4 (top row), NaCl (middle row), and NaSCN (bottom row) concentration. Different symbols indicate different salt concentrations and ionic strengths as codified by their inverse Debye length κ. The plots for each type of salt are presented in rows where pH values run from 6.0 (left column), 7.0 (middle column), and 8.3 (right column). A model of hard-sphere excluded volume repulsion, with no attractive interactions is shown for reference as a black solid line.

visualization. We first obtained the triangulated SAS representation of the amino acid group atoms lying on that surface. These triangulated mesh surface atomic points were then mapped onto the circumscribed sphere of radius R. The radius R from the protein center of mass (COM)[47] is defined in such a way that it encloses the farthest point on the protein SAS. The IgG1 mAb model structure used to construct this mapping is based on the 3.2 Å resolution X-ray crystallography[77] but allows for the additional relaxation due to the hinge-region flexibility.[68] This leads to an asymmetric shape

DOI: 10.1021/acs.jpcb.5b02459
J. Phys. Chem. B XXXX, XXX, XXX−XXX

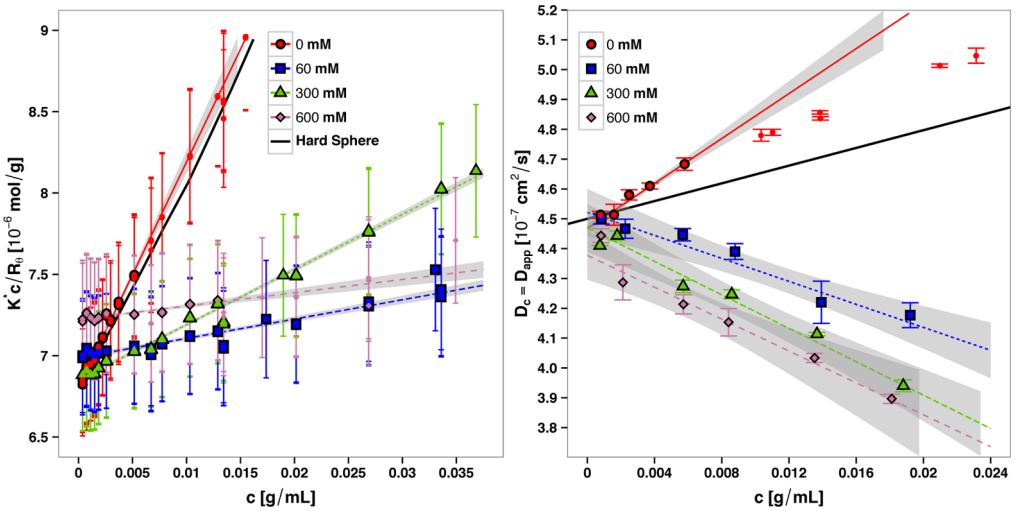

Figure 3. Concentration dependence of Debye plots of scattering ratio $K^* c/R_\theta$ (left) and collective diffusivities D_c as apparent diffusion (right) at pH = 6.0 with varying NaCl concentration. Different symbols indicate different salt concentrations. Linear fits are obtained using eqs 1 and 3. The concentration range in which the fitting was performed is presented as larger points with the background. The confidence intervals of linear fits are shown with gray bands. A model of hard-sphere excluded volume repulsion, with no attractive interactions and thus no-screening is shown for reference as a black solid line.

that has a three-lobe projection onto the circumscribed spherical surface with low symmetry, see Figure 1 (bottom row). Even though this mapping provides the coordinates of amino acid charges on the spherical surface, these discrete data do not give a visually clear insight into the 3D nature of the charge distribution. We obtain a more informative visual representation by using a smeared charge distribution obtained by assigning to each atomic partial charge of the residue a scalar Gaussian density with the width parameter W = 5 Å, specifying the spatial extent of the density. The total charge density field is then constructed by summing the scalar densities of all the contributing charges. Finally, in order to avoid overlaps and to show simultaneously the total charge density over the whole spherical surface, we represent the surface in the Mollweide projection having the polar and the azimuthal angle as the coordinate axes.[78,79]

The top and bottom row of Figure 1 thus represent two different features of the protein electrostatics. Although the first one allows visualization of the solution charge redistribution in the presence of the protein charges, the latter allows the visualization of the underlying protein charges themselves, without any induced changes in the solution charge distribution.

The asymmetric three-lobe form of the Mollweide projection onto the circumscribed sphere is also preserved for charge distribution at all values of the solution pH, see Figure 1, being most inconspicuous close to the IEP, located at pH ∼ 8. It is also clear from comparing the surface charge distribution at pH = 7.0 to that close to the IEP, that it exhibits not only a patchy monopolar charge distribution but actually shows a distinctive dipolar component due to charge distribution of both signs. It could be worthwhile to actually quantify the charge distribution on the circumscribed sphere into various multipolar components, not completely dissimilar to the procedure introduced recently by Hoppe[49] (see Discussion). However, it seems that this decomposition would be beneficial to calculate the electrostatic interactions between patchy protein surfaces only if they exhibit a certain point group symmetry.[78] While this symmetry is readily available in the context of proteinaceous viral shell aggregates, it is usually completely lacking for single proteins in general and for IgG1 mAb in particular.

The multipolar decomposition would therefore not provide an additional simplification to an accurate calculation of the electrostatic part of the interaction between patchy charged protein surfaces. Nevertheless, we believe that the projection of the charge density onto the protein circumscribed sphere provides a better representation of the anisotropic charge distribution then simple color-maps of the solvent-accessible surface of the protein.

RESULTS

Concentration-series-dependent light-scattering experiments were conducted over the pH range of 6.0, 7.0, and 8.3 under conditions of low to high buffer ionic strength due to uniunivalent NaCl, NaSCN, and unidivalent Na_2SO_4 solution of varying salt concentration between 60 and 600 mM. These pH values were chosen in order to investigate the pH range from net negative surface charge at pH = 6.0, all the way to high-surface charge anisotropy at pH = 7.0 and 8.3 near mAb's IEP point (see Figure 1) as well as to complement the recent results obtained by Roberts et al.[26]

The ionic strength of the buffer was set at I = 20 mM, a value small enough in order to minimize the effect of buffer on the ionic screening and large enough to buffer the solution pH. In this pH range, the phosphate ions are in a divalent state (with small amount of mono- and trivalent states) and specific effect from the phosphate ion can contribute to investigated conditions.[80]

Although this pH range was not investigated exhaustively in our previous study[9] due to technique limitations, the real reason for its consideration is due to the fact that in these conditions the mAb protein surface charge distribution shows the strongest anisotropy and inhomogeneities as is clear from our model calculations presented in Figure 1. The salt types were chosen to accentuate the Hofmeister series effects: from the most "chaotropic" SCN^-, through the middle of the series with Cl^- to the most "cosmotropic" SO_4^{2-} ion.[26,81] A less empirical description of the Hofmeister effect would need to be

DOI: 10.1021/acs.jpcb.5b02459
J. Phys. Chem. B XXXX, XXX, XXX−XXX

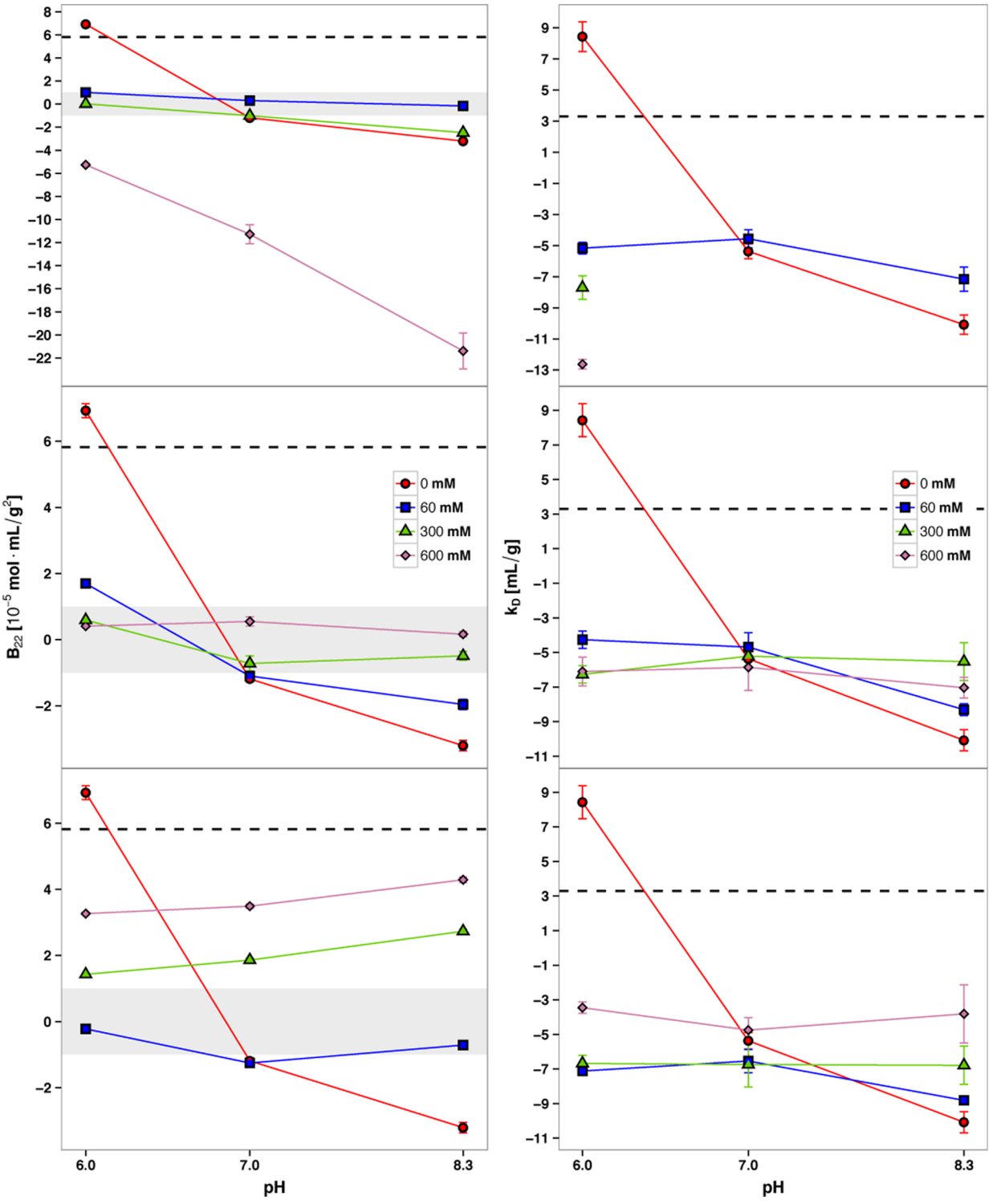

Figure 4. pH dependence of second virial coefficient B_{22} (left) and diffusion interaction coefficient k_D (right) with varying Na_2SO_4 (top row), NaCl (middle row), and NaSCN (bottom row) concentration. The lines are shown solely to guide the eyes. Different symbols indicate different salt concentrations. The gray bands (left) show FOM values for statistically insignificant values between −1 and +1 × 10^{-5} mol·mL/g^2. B_{22} for a hard-sphere excluded volume repulsion model is shown for reference as a black horizontal dashed line. k_D values for 300 and 600 mM Na_2SO_4 salt concentrations at pH 7 and 8.3 are not shown because they did not passed PdI limit criteria for monodisperse samples.

based on a proper parametrization of the molecular interaction of the various ion types with amphiphillic charged surfaces and is still lacking.[82] Although in the case of polypeptides this parametrization is not available, recent advances in the microscopic understanding of the Hofmeister effect in the surface tension (see refs 24,25,83 and references therein) do actually allow to arrange the various ions in that case into an extended reverse Hofmeister series with decreasing adhesivity strength at the solution interface.[83] The anion partial Hofmeister series in the case of the surface tension of electrolyte solutions is then obtained as $F^-(\sim SO_4^{2-}) > IO_3^- > Cl^- > ClO_3^- \gg I^- > ClO_4^- > SCN^-$, while the cation

DOI: 10.1021/acs.jpcb.5b02459
J. Phys. Chem. B XXXX, XXX, XXX−XXX

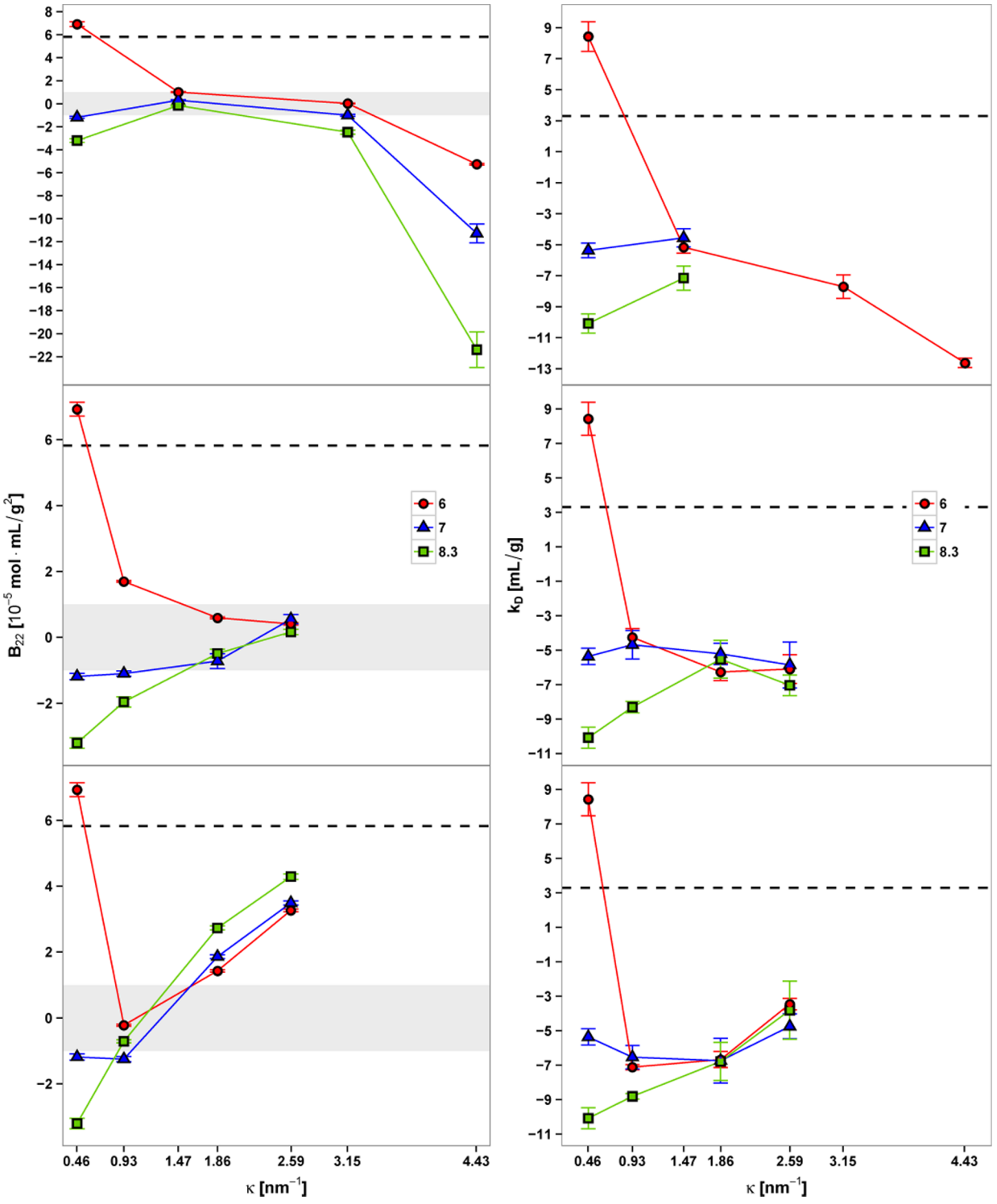

Figure 5. Screening parameter κ dependence of second virial coefficient B_{22} (left) and diffusion interaction coefficient k_D (right) with varying Na_2SO_4 (top row), NaCl (middle row), and NaSCN (bottom row) concentration. The lines are shown solely to guide the eyes. Different symbols indicate different salt concentrations. In graphs of B_{22}, the gray bands show FOM values for statistically insignificant values between −1 and +1 × 10^{-5} mol·mL/g^2. A model of hard-sphere excluded volume repulsion value, with no attractive interactions is shown for reference as a black horizontal dashed line. The k_D values for 300 and 600 mM Na_2SO_4 salt concentraions at pH 7 and 8.3 are not shown because they did not pass the PdI limit criteria for monodisperse samples.

Hofmeister series is given by $K^+ > Na^+ > H^+$. The Hofmeister effect appears to be substantially stronger for anions, possibly connected with the stronger van der Waals forces related to the large anion polarizabilities,[84] and has SO_4^{2-} and SCN^- at the opposite sides of the series. We thus assume that the ion-specific effects that we will measure are somehow maximized.

First, we report Rayleigh scattering data R_θ/K^* versus protein concentration for various pH and ionic strengths for selected screening parameters κ and a hard sphere reference

DOI: 10.1021/acs.jpcb.5b02459
J. Phys. Chem. B XXXX, XXX, XXX−XXX

system to determine the effects of Na_2SO_4, NaCl and NaSCN on the protein−protein interactions of mAb (Figure 2). We assume monodisperse mAbs, interacting with nonspecific protein−protein interactions and compare the measured values with a reference hard-core excluded volume system.

We observe a linear dependence of R_θ/K^* versus concentration in the limit of small concentrations. Deviations set in at larger values of the protein concentration, (>100 mg/mL), where the linear virial expansion of the osmotic pressure is no longer valid. In this regime, the measured concentration dependence of the Rayleigh ratio indicates that the reference hard-core excluded volume system is a poor approximation and additional, mostly repulsive interactions come into play, dependent on the pH, the ionic strength, and the salt type of the solution.

After determination of the linear concentration range, the analysis of the mAb scattering signals was used to estimate B_{22} and k_D using eq 1 and 3 following the same procedure as in our previous study.[9] As an example of the linear regime, the data is presented as Debye plots of scattering ratio $K^*\ c/R_\theta$ together with collective diffusivities D_C as apparent diffusion constant at pH = 6.0 with varying NaCl concentration (Figure 3).

From these results (Figure 3), it can be seen that the validity of the linear regime varies depending on the mAb interaction potential behavior arising from different solution conditions.[34] The nonlinearity was reported even at the concentration range where the linearity was expected from our study.[85] For a more concentrated solution, the linear analysis using the second virial coefficient is obviously not suitable for quantification of the interactions, and one would have to take recourse to more sophisticated methods involving new approximations.[86] The most pronounced deviation of the SLS Debye plot as well as DLS collective diffusivity plot from linearity is seen expectedly at no-salt conditions and thus no-screening for pH = 6 in NaCl, remaining nevertheless close to the hard-sphere interaction second virial coefficient estimate. This too is not surprising because "no-salt" condition interactions, while long-range, are still consistently repulsive.

The intersections of the linear fits with the ordinate give the molecular weight M and infinite-dilution diffusion coefficients D_0 together with the hydrodynamic radius r_H in the case of the SLS method or the DLS method, respectively. The data do not collapse to a single value but depend on the salt concentration. D_0 seems to have a small ionic strength dependence in the case of NaCl and a more pronounced dependence for NaSCN and Na_2SO_4 salt types.

The dependence of M on concentration is at least in part due to the change in the differential refractive index of the protein solution dn/dc but remains in general small.[87] Additionally, it can also arise from the changes in the surface charging/adsorption equilibrium either of the mobile ions or possibly the charged impurities in the solution, an effect that was not yet investigated systematically. Because the DLS intercepts do not depend on the absolute refractive index, we can conclude that their variation stemms possibly from the interaction of solution ions with the protein molecule.[80] The salt dependence of the diffusion coefficient for highly charged colloidal particles in the limit of constant surface potential was explained more precisely in our previous work.[9] The quantitative understanding of the solvent structure effects[80,87,88] can be attributed to the strong hydration interactions at separations ∼1 nm.

Quantitative extraction of the osmotic second virial coefficients B_{22} from the dilute regime of light scattering experiments are presented for each cosolute system (Figure 4). We compare the virial coefficient values for different solution conditions with the estimated value of the hard-sphere repulsion virial coefficient B_{22}^{HS}, as this allows one to gauge the relative importance of long-range soft attractions and repulsions referenced to the magnitude of the steric repulsion contribution.[34,86,89] If $B_{22} \geq B_{22}^{HS}$, the soft repulsive interactions tend to dominate the short-range steric interaction, whereas in the opposite case of $B_{22} \leq B_{22}^{HS}$, the soft attractive interaction tends to diminish the effect of the short-range steric repulsion. We see that mostly the latter case is applicable to experimental data in Figure 4.

Before proceeding to the SLS virial coefficient and the DLS interaction parameter data, we note that only small, uncorrelated changes of mAb1 molecular mass at infinite dilution are observed, indicating that the interactions mediated by the NaCl, NaSCN, and Na_2SO_4 are weak in nature. The weakness of the molecular mass variation indicates that the simplified treatment of these many-component systems as two component solutions is a reasonable approximation. The cosolutes can then be treated as part of the solvent matrix but are recognized as the modifying components of the aqueous solution, when differences between protein−protein interactions become apparent.

The measured values of B_{22} show substantial variation with respect to pH, Figure 4, as well as the screening parameter, Figure 5, of the electrolyte solution environment. The pH dependencies, Figure 4, are very ion-specific and show scarcely any universal behavior. In the case of Na_2SO_4, the second virial coefficient shows a modest decrease with pH, except for the largest salt concentration of 600 mM, where it follows a reverse trend toward substantially more negative values. This would indicate that for large pH and intermediate to small salt concentration the interactions are becoming more attractive as the screening is increased, implying furthermore that the attraction is due either to short-range interactions or is a consequence of the underlying van der Waals attraction, once the repulsion is attenuated by screening (see Discussion and Conclusions). In the case of NaCl, the situation is different and in the zero-salt-added case, we observe the most pronounced variation of the second virial coefficient with pH, decreasing from large positive values to moderate negative values. This again indicates either an enhancement in attractive interactions or an attenuation of the repulsive interactions. Because the effect is largest for small salt concentrations, it can be assumed that it is electrostatic in nature, possibly stemming from the attractions due to the inhomogeneous distribution of protein surface charge or fluctuations in the ionic atmosphere, see Figure 1, with a pronounced charge inhomogeneity in the pH = 7.0−8.3 region. To some extent the NaSCN data tell a similar story: for vanishing salt concentration the second virial coefficient goes from large positive values to moderate negative values. Again this could possibly reflect the growing charge inhomogeneity on increase of the pH. However, for larger values of salt concentration the trend is exactly reversed, giving rise to significantly larger repulsions on increase of pH, persistent even in the case of pronounced screening. A possible rationalization would be a specific adsorption of the hydrated salt ions to the protein surface, contributing to a larger effective diameter of the protein that shows as a moderate increase in repulsion, even if the long-range electrostatic interactions are completely screened out.

DOI: 10.1021/acs.jpcb.5b02459
J. Phys. Chem. B XXXX, XXX, XXX−XXX

What is furthermore important to notice is that there is a reversal in the Hofmeister effect for pH above and below the IEP, estimated to be at pH $\simeq$ 8 for this protein, as the salt concentration varies. Our results add to the list of proteins showing such behavior, as described in refs 84,90−92. For low salt at pH = 6, Na_2SO_4 shows a larger second virial coefficient then NaSCN, indicating either a larger repulsion or a smaller attraction, while at the opposite extreme of high salt at pH = 8.3, Na_2SO_4 shows a much more pronounced attraction then NaSCN. The rationalization of this reverse Hofmeister ion ordering is rather difficult to understand, though attempts abound, implicating either the van der Waals interactions between the solution ions and charged surfaces or surface-modified ion hydration interactions[93,94] or indeed the Kirkwood−Shumaker interaction,[95] see the Discussion and Conclusions section for more details.

To explain the electrostatic contribution to this effect, the low salt concentration data points should be considered, where the screening of electrostatic interactions is smallest. Increasing the salt in all three cases from 0 to 60 mM leads to the same second virial coefficient and diffusion interaction coefficient behavior. At low pH, there is a decrease in the second virial coefficient, at intermediate pH, there is no change, and at high pH, there is an increase in the second virial coefficient for all three salt types. The ion specific effects are much more clearly manifested at higher salt concentrations, and they seem to follow the standard Hofmeister series, where sulfate is most effective at salting-out and thiocyanate is least effective at salting-out. At 300 and 600 mM salt concentration, the salt screening is pronounced, inducing a slight reversal of the Hofmeister series effect, if one compares the thiocyanate results at 60 mM and pH 6 to the chloride result, indicating more attractive effective interactions in thiocyanate. Also, it appears that at high pH the salting-in effects in thiocyanate and the salting-out effects of sulfate are most pronounced.

In the case of ionic strength variation of B_{22}, Figure 5, the case of NaCl is closest to what one would expect purely on the DLVO grounds: as the long-range electrostatic interaction is screened, the absolute value of the second virial coefficient levels off to zero. Clearly in the case of small screening at pH = 6 the repulsion is dominant, while attraction is dominant for pH = 8.3. A possible rationalization of this would be the effect of the inhomogeneous charge distribution that could lead to attraction between oppositely charged patches on the surfaces of the interaction proteins, attenuated by the presence of screening, or indeed the ionic atmosphere fluctuations close to the IEP, that would contribute an additional strong attraction (see Discussion and Conclusions). The cases of Na_2SO_4 and NaSCN provide variations on this background but in the opposite direction. Na_2SO_4 shows a general trend toward more negative second virial coefficient on increase of screening, except in the case of pH = 6. In that case, the trend is exactly opposite: intermediate negative values of the second virial coefficient tend to zero for intermediate values of screening. NaSCN shows a pronounced growth toward positive values except for the smallest investigated value of pH. In that case, the second virial coefficient first drops and then increases again for more pronounced electrostatic screening. Although in the case of Na_2SO_4 one could envision a progress toward short-range attractions of a general van der Waals type, the NaSCN case indicates an adsorption of the solution ions that would change the effective hard-sphere diameter of the protein contributing to an enhanced short-range repulsion in the strong screening regime.

As already pointed out, on general grounds, the diffusion interaction coefficient k_D, though obtained from a different experiment, is expected to trail the behavior of the second virial coefficient. The data on Figure 4 and Figure 5, for the cases where the comparison is possible, in general corroborate these expectations if we take into account that the connection between the two quantitites is not trivial. The general trends nevertheless coincide. This is the case for the pH dependence of k_D at a fixed ionic strength of the solution or for the ionic strength dependence at a fixed value of pH. While the direct dependence of k_D on the interaction parameters can be calculated,[9] it is however based on additional assumptions and has a weaker status than the straightforward connection between k_D and the second virial coefficient.

DISCUSSION AND CONCLUSIONS

In order to understand our data, even on a qualitative level, the DLVO framework with repulsive screened electrostatic interactions and partially screened attractive van der Waals interactions appears to be highly deficient.[96,97] By partially screened van der Waals interactions, we understand the fact that in the Lifshitz theory, the zero frequency term in the Matsubara sum of the Hamaker coefficient is screened with twice the inverse Debye screening length.[17] As in aqueous solutions, the zero frequency term in the Matsubara sum can contribute more than one-half to the total strength of the van der Waals interactions, the overall effect of the salt screening should lead to a drastic screening of electrostatic repulsion and a moderate attenuation of the van der Waals attraction. This should be the canonical expectation, if there were no other ion-specific effects in the interaction between solution ions and the charged macroions.

However, in the case of protein−protein interactions one would in fact need to upgrade the DLVO theory by including also the Kirkwood−Schumaker (KS) interactions that contribute to the attractive interactions in the vicinity of the IEP (for details see refs 95,98,99). The KS interaction stems from the ionic cloud fluctuations due to charge regulation of the amino acids at the protein surface[96] and is proportional to the square of the capacitance of the protein charge distribution (see below). By charge regulation, we mean the dependence of the dissociation equilibria of the amino acids on the surface of the protein on local solution parameters: pH, salt concentration, salt type, dielectric discontinuities, presence of other vicinal dissociation groups, and so forth.[96,100,101] Charge regulation in fact introduces pronounced pH effects in the strength of the electrostatic interactions that are not available within the standard DLVO theory.[102] The KS interaction is longer-ranged then the van der Waals interaction but acts only in the vicinity of the IEP of the protein, and it could thus contribute to an additional destabilization of the protein solution as it goes through the IEP either in the salt concentration or the pH parameter regions.

Charge regulation introduces also an important modification in the generally recognized patchiness of the protein charge distribution, which is in some respects quite similar to the patchiness in the case of complex colloids. However, contrary to the case of patchy colloids, where the patchiness can be chemically controlled, quantified, and modeled,[103,104] for proteins in general, no such simple quantification and modeling of the charge patchiness is available. As a simple point of

DOI: 10.1021/acs.jpcb.5b02459
J. Phys. Chem. B XXXX, XXX, XXX−XXX

illustration, we have shown the variation in the surface charge patchiness as well as the solution mobile charge response for the IgG1 monoclonal antibody at various solution conditions in Figure 1 for pH = 6.0, 7.0, and 8.3. For proteins, charge and shape inhomogeneities are obviously intricately connected: patchiness is thus partly geometric and partly electrostatic. Our attempt to disentangle them is contained in going from the upper to lower row in Figure 1, by projecting the protein surface charge, not the PB distributed mobile space charge, from the protein solvent accessible surface onto a circumscribed spherical surface, where it is then visualized in the Mollweide projection.

Charge patchiness can affect also the protein−protein interactions[105,106] and is further complicated by charge regulation that leads to coupling with solution conditions (pH, ionic strength) as well ion-specific effects leading to patch-charge regulation. Furthermore, for highly symmetric surfaces, such as proteinaceous virus capsids, the orientation effect can be easily quantified through certain point group symmetries that lead to orientation dependent electrostatic interactions.[78] No such simple characterization is possible for highly irregular protein surfaces. As the various amino acids go through their dissociation states, they pattern the solution-exposed surface of the protein, conferring to it variously shaped, irregular charge decorations that can be represented and quantified for large separations as its orientation-dependent multipolar moment terms in the interaction potential $w(r, \Omega)$.[49,107] The angular average, $<\cdots>_\Omega$, of this potential, that enters also the second virial coefficient to the lowest order, can be written explicitly in the limit of large separations[107] and leads to an effective separation-dependent attractive potential of the form

$$<w(r, \Omega)>_\Omega = -\alpha_{e\mu}^2\left(\frac{e^{-\kappa R}}{R^2}\right)^2 - \alpha_{\mu\mu}^2\left(\frac{e^{-\kappa R}}{R^3}\right)^2 + \ldots \quad (5)$$

where R is the separation between two proteins. Here $\alpha_{e\mu}$ and $\alpha_{\mu\mu}$ indicate orientationally averaged charge-dipole and dipole−dipole parts of the interaction potential, respectively. Clearly on the lowest order approximation this multipolar expansion of the protein charge distribution decays with half the Debye length, having also a long-range tail of R^{-4}. The $\alpha_{\mu\mu}$ part of the effective separation dependent potential, decaying as a screened sixth power fo the separation, obviously pertains to van der Waals interactions and could be in fact included into the zero frequency Matsubara term.[17]

Apart from the orientational contributions as described above, the KS interactions too make their mark on the attractive part of the interaction potential close to the IEP. In the same limit of large separations as in eq 5, the KS interaction assumes the form:[98,99]

$$w(r) \approx -C^2\left(\frac{e^{-\kappa R}}{R}\right)^2 \quad (6)$$

being proportional to the square of the macroion capacitance C, which in its turn follows from the charge variance

$$C = <(q - <q>)^2> = -\frac{1}{\ln 10}\frac{\partial q(\mathrm{pH})}{\partial \mathrm{pH}} \quad (7)$$

Here $q(\mathrm{pH})$ is the pH (as well as salt, ion type, etc.) dependent charge of the protein. Obviously, the KS potential is longer ranged then any of the orientationaly averaged multipolar terms in eq 5 and should thus be among the important sources of the pH dependent attractive contributions to the protein−protein interaction potential. This would remain true even at pronounced screening since the second virial coefficient is a global property, depending on an integral of the interaction over all separations and a substantial contribution even if limited to only small separation would add to it. Clearly, the standard multipolar effects, dependent on the multipolar moments of the charge distribution would be subdominant to the KS interaction also in terms of possibly explaining the pH and ion specific effects seen in our experiments.

An additional observation worth noting in the charge projection, Figure 1, is that not only is there patchiness in the monopolar charge distribution, clearly seen on panes (a) and (c) (lower row), but also patchiness in the dipolar charge distribution, seen most clearly on pane (b). This local dipolar patchiness is different from the global dipolar moment of the protein charge distribution,[49,107] and its consequences have not been explored yet. At pronounced screening conditions, the remaining short-range part of this dipolar patchiness distribution could show a residual effect in the interaction potential, possibly contributing to the observed trend toward negative second virial coefficients with increased screening that can obviously not be rationalized within the DLVO paradigm.

In addition, charge regulation of the proteins surface, which lies at the basis of the patchiness and fluctuation interactions of the KS type, is prone to ion-specific effects because it relies on the details of the dissociation equilibrium that depend not only on the charge of the solution ions but also on other details of their structure such as polarizability, short-range interaction with the protein surface, and so forth[24,93,94,108] As the nature of ion specific effects is far from being adequately understood,[109] there is no definitive interpretation one can give to the ion specific effects. We clearly see them in our experiments together with the fact that they are related to the nature of the anion, but we cannot say with any certainty what they are due to and/or properly quantify them in terms of well understood interaction parameters.

AUTHOR INFORMATION

Corresponding Author

*E-mail: dejan.arzensek@gmail.com.

Notes

The authors declare no competing financial interest.

ACKNOWLEDGMENTS

This work was financed in part by the European Union, European Social Fund, within the framework of the Operational Programme for Human Resources Development for the Period 2007-2013. R.P. acknowledges support of ARRS through research program P1-0055 and research project J1-4297. D.A. gratefully acknowledges Sophia Kenrick (Wyatt Technologies, Santa Barbara, California) for insightful discussions and her support in data analysis.

REFERENCES

(1) Leckband, D.; Sivasankar, S. Forces controlling protein interactions: theory and experiment. *Colloids Surf., B* **1999**, *14*, 83−97.

(2) French, R. H.; Parsegian, V. A.; Podgornik, R.; Rajter, R. F.; Jagota, A.; Luo, J.; Asthagiri, D.; Chaudhury, M. K.; Chiang, Y.-m.; Granick, S.; et al. Long range interactions in nanoscale science. *Rev. Mod. Phys.* **2010**, *82*, 1887−1944.

DOI: 10.1021/acs.jpcb.5b02459
J. Phys. Chem. B XXXX, XXX, XXX−XXX

(3) Verwey, E. J. W.; Overbeek, J. T. G. *Theory of the Stability of Lyophobic Colloids: The Interaction of Sol Particles Having an Electric Double Layer*; Elsevier Publishing Company: Amsterdam, 1948.
(4) Bishop, K. J. M.; Wilmer, C. E.; Soh, S.; Grzybowski, B. A. Nanoscale forces and their uses in self-assembly. *Small* **2009**, *5*, 1600−1630.
(5) Nel, A. E.; Mädler, L.; Velegol, D.; Xia, T.; Hoek, E. M. V.; Somasundaran, P.; Klaessig, F.; Castranova, V.; Thompson, M. Understanding biophysicochemical interactions at the nano-bio interface. *Nat. Mater.* **2009**, *8*, 543−557.
(6) Prausnitz, J. The fallacy of misplaced concreteness. *Biophys. J.* **2015**, *108*, 453−454.
(7) Leavy, O. Therapeutic antibodies: past, present and future. *Nat. Rev. Immunol.* **2010**, *10*, 297−297.
(8) Shire, S. J.; Shahrokh, Z.; Liu, J. Challenges in the development of high protein concentration formulations. *J. Pharm. Sci.* **2004**, *93*, 1390−1402.
(9) Arzenšek, D.; Kuzman, D.; Podgornik, R. Colloidal interactions between monoclonal antibodies in aqueous solutions. *J. Colloid Interface Sci.* **2012**, *384*, 207−216.
(10) Roberts, D.; Keeling, R.; Tracka, M.; van der Walle, C. F.; Uddin, S.; Warwicker, J.; Curtis, R. The role of electrostatics in protein-protein interactions of a monoclonal antibody. *Mol. Pharmaceutics* **2014**, *11*, 2475−2489.
(11) Esfandiary, R.; Parupudi, A.; Casas-Finet, J.; Gadre, D.; Sathish, H. Mechanism of reversible self-association of a monoclonal antibody: role of electrostatic and hydrophobic interactions. *J. Pharm. Sci.* **2015**, *104*, 577−586.
(12) Saito, S.; Hasegawa, J.; Kobayashi, N.; Kishi, N.; Uchiyama, S.; Fukui, K. Behavior of monoclonal antibodies: relation between the second virial coefficient (B (2)) at low concentrations and aggregation propensity and viscosity at high concentrations. *Pharm. Res.* **2012**, *29*, 397−410.
(13) Israelachvili, J. N. *Intermolecular and Surface Forces: Revised*, 3rd ed.; Academic Press: San Diego, CA, 2011.
(14) Piazza, R. Protein interactions and association: an open challenge for colloid science. *Curr. Opin. Colloid Interface Sci.* **2004**, *8*, 515−522.
(15) Neal, B.; Asthagiri, D.; Lenhoff, A. Molecular origins of osmotic second virial coefficients of proteins. *Biophys. J.* **1998**, *75*, 2469−2477.
(16) Velev, O. D.; Kaler, E. W.; Lenhoff, A. M. Protein interactions in solution characterized by light and neutron scattering: comparison of lysozyme and chymotrypsinogen. *Biophys. J.* **1998**, *75*, 2682−2697.
(17) Parsegian, V. A. *Van der Waals Forces: A Handbook for Biologists, Chemists Engineers, and Physicists*; Cambridge University Press: New York, 2005.
(18) Liang, Y.; Hilal, N.; Langston, P.; Starov, V. Interaction forces between colloidal particles in liquid: theory and experiment. *Adv. Colloid Interface Sci.* **2007**, *134*−*135*, 151−166.
(19) Kunz, W. *Specific Ion Effects*; World Scientific: Singapore, 2009.
(20) Ahamed, T.; Esteban, B. N. A.; Ottens, M.; van Dedem, G. W. K.; van der Wielen, L. A. M.; Bisschops, M. A. T.; Lee, A.; Pham, C.; Thömmes, J. Phase behavior of an intact monoclonal antibody. *Biophys. J.* **2007**, *93*, 610−619.
(21) Lewus, R. A.; Darcy, P. A.; Lenhoff, A. M.; Sandler, S. I. Interactions and phase behavior of a monoclonal antibody. *Biotechnol. Prog.* **2011**, *27*, 280−289.
(22) Dumetz, A. C.; Chockla, A. M.; Kaler, E. W.; Lenhoff, A. M. Protein phase behavior in aqueous solutions: crystallization, liquid-liquid phase separation, gels, and aggregates. *Biophys. J.* **2008**, *94*, 570−583.
(23) Levin, Y. Polarizable ions at interfaces. *Phys. Rev. Lett.* **2009**, *102*, 147803.
(24) Ben-Yaakov, D.; Andelman, D.; Podgornik, R.; Harries, D. Ion-specific hydration effects: extending the Poisson-Boltzmann theory. *Curr. Opin. Colloid Interface Sci.* **2011**, *16*, 542−550.
(25) Markovich, T.; Andelman, D.; Podgornik, R. Surface tension of electrolyte solutions: a self-consistent theory. *EPL Europhys. Lett.* **2014**, *106*, 16002.
(26) Roberts, D.; Keeling, R.; Tracka, M.; van der Walle, C. F.; Uddin, S.; Warwicker, J.; Curtis, R. Specific ion and buffer effects on protein-protein interactions of a monoclonal antibody. *Mol. Pharmaceutics* **2015**, *12*, 179−193.
(27) Liu, J.; Nguyen, M. D.; Andya, J. D.; Shire, S. J. Reversible self-association increases the viscosity of a concentrated monoclonal antibody in aqueous solution. *J. Pharm. Sci.* **2005**, *94*, 1928−1940.
(28) Yadav, S.; Liu, J.; Shire, S. J.; Kalonia, D. S. Specific interactions in high concentration antibody solutions resulting in high viscosity. *J. Pharm. Sci.* **2010**, *99*, 1152−1168.
(29) Yadav, S.; Shire, S. J.; Kalonia, D. S. Viscosity analysis of high concentration bovine serum albumin aqueous solutions. *Pharm. Res.* **2011**, *28*, 1973−1983.
(30) Yadav, S.; Shire, S. J.; Kalonia, D. S. Viscosity behavior of high-concentration monoclonal antibody solutions: correlation with interaction parameter and electroviscous effects. *J. Pharm. Sci.* **2012**, *101*, 998−1011.
(31) Salinas, B. A.; Sathish, H. A.; Bishop, S. M.; Harn, N.; Carpenter, J. F.; Randolph, T. W. Understanding and modulating opalescence and viscosity in a monoclonal antibody formulation. *J. Pharm. Sci.* **2010**, *99*, 82−93.
(32) Yadav, S.; Shire, S. J.; Kalonia, D. S. Factors affecting the viscosity in high concentration solutions of different monoclonal antibodies. *J. Pharm. Sci.* **2010**, *99*, 4812−4829.
(33) Chari, R.; Jerath, K.; Badkar, A. V.; Kalonia, D. S. Long- and short-range electrostatic interactions affect the rheology of highly concentrated antibody solutions. *Pharm. Res.* **2009**, *26*, 2607−2618.
(34) Sahin, E.; Grillo, A. O.; Perkins, M. D.; Roberts, C. J. Comparative effects of pH and ionic strength on protein-protein interactions, unfolding, and aggregation for IgG1 antibodies. *J. Pharm. Sci.* **2010**, *99*, 4830−4848.
(35) Kanai, S.; Liu, J.; Patapoff, T. W.; Shire, S. J. Reversible self-association of a concentrated monoclonal antibody solution mediated by Fab-Fab interaction that impacts solution viscosity. *J. Pharm. Sci.* **2008**, *97*, 4219−4227.
(36) Saito, S.; Hasegawa, J.; Kobayashi, N.; Tomitsuka, T.; Uchiyama, S.; Fukui, K. Effects of ionic strength and sugars on the aggregation propensity of monoclonal antibodies: influence of colloidal and conformational stabilities. *Pharm. Res.* **2013**, *30*, 1263−1280.
(37) Scherer, T. M. Cosolute effects on the chemical potential and interactions of an IgG1 monoclonal antibody at high concentrations. *J. Phys. Chem. B* **2013**, *117*, 2254−2266.
(38) Yadav, S.; Sreedhara, A.; Kanai, S.; Liu, J.; Lien, S.; Lowman, H.; Kalonia, D.; Shire, S. Establishing a link between amino acid sequences and self-associating and viscoelastic behavior of two closely related monoclonal antibodies. *Pharm. Res.* **2011**, *28*, 1750−1764.
(39) Yadav, S.; Laue, T. M.; Kalonia, D. S.; Singh, S. N.; Shire, S. J. The influence of charge distribution on self-association and viscosity behavior of monoclonal antibody solutions. *Mol. Pharmaceutics* **2012**, *9*, 791−802.
(40) Chaudhri, A.; Zarraga, I. E.; Kamerzell, T. J.; Brandt, J. P.; Patapoff, T. W.; Shire, S. J.; Voth, G. A. Coarse-grained modeling of the self-association of therapeutic monoclonal antibodies. *J. Phys. Chem. B* **2012**, *116*, 8045−8057.
(41) Chaudhri, A.; Zarraga, I. E.; Yadav, S.; Patapoff, T. W.; Shire, S. J.; Voth, G. A. The role of amino acid sequence in the self-association of therapeutic monoclonal antibodies: insights from coarse-grained modeling. *J. Phys. Chem. B* **2013**, *117*, 1269−1279.
(42) Lapelosa, M.; Patapoff, T. W.; Zarraga, I. E. Molecular simulations of the pairwise interaction of monoclonal antibodies. *J. Phys. Chem. B* **2014**, *118*, 13132−13141.
(43) Lilyestrom, W. G.; Yadav, S.; Shire, S. J.; Scherer, T. M. Monoclonal antibody self-association, cluster formation, and rheology at high concentrations. *J. Phys. Chem. B* **2013**, *117*, 6373−6384.
(44) Sarangapani, P. S.; Hudson, S. D.; Migler, K. B.; Pathak, J. A. The limitations of an exclusively colloidal view of protein solution hydrodynamics and rheology. *Biophys. J.* **2013**, *105*, 2418−2426.

DOI: 10.1021/acs.jpcb.5b02459
J. Phys. Chem. B XXXX, XXX, XXX−XXX

(45) Gögelein, C.; Nägele, G.; Tuinier, R.; Gibaud, T.; Stradner, A.; Schurtenberger, P. A simple patchy colloid model for the phase behavior of lysozyme dispersions. *J. Chem. Phys.* **2008**, *129*, 085102.
(46) Kurut, A.; Persson, B. A.; Åkesson, T.; Forsman, J.; Lund, M. Anisotropic interactions in protein mixtures: self assembly and phase behavior in aqueous solution. *J. Phys. Chem. Lett.* **2012**, *3*, 731−734.
(47) Chan, H. Y.; Lankevich, V.; Vekilov, P. G.; Lubchenko, V. Anisotropy of the coulomb interaction between folded proteins: consequences for mesoscopic aggregation of lysozyme. *Biophys. J.* **2012**, *102*, 1934−1943.
(48) Elcock, A. H.; McCammon, J. A. Calculation of weak protein-protein interactions: the ph dependence of the second virial coefficient. *Biophys. J.* **2001**, *80*, 613−625.
(49) Hoppe, T. A simplified representation of anisotropic charge distributions within proteins. *J. Chem. Phys.* **2013**, *138*, 174110.
(50) Postarnakevich, N.; Singh, R. *Proceedings of the 2009 ACM Symposium on Applied Computing*; ACM: New York, 2009; pp 782−787.
(51) Berne, B. J.; Pecora, R. *Dynamic Light Scattering: With Applications to Chemistry, Biology, and Physics*; Courier Dover Publications: Mineola, MN, 2000.
(52) Muschol, M.; Rosenberger, F. Interactions in undersaturated and supersaturated lysozyme solutions: Static and dynamic light scattering results. *J. Chem. Phys.* **1995**, *103*, 10424−10432.
(53) Some, D., Kenrick, S. *Characterization of Protein-Protein Interactions via Static and Dynamic Light Scattering*; Cai, J., Wang, R. E., Eds.; InTech: Rijeka, Croatia, **2012**; pp 401−426.
(54) Zimm, B. H. The scattering of light and the radial distribution function of high polymer solutions. *J. Chem. Phys.* **1948**, *16*, 1093−1099.
(55) Ma, Y.; Acosta, D. M.; Whitney, J. R.; Podgornik, R.; Steinmetz, N. F.; French, R. H.; Parsegian, V. A. Determination of the second virial coefficient of bovine serum albumin under varying pH and ionic strength by composition-gradient multi-angle static light scattering. *J. Biol. Phys.* **2015**, *41*, 85−97.
(56) Scherer, T. M.; Liu, J.; Shire, S. J.; Minton, A. P. Intermolecular interactions of IgG1 monoclonal antibodies at high concentrations characterized by light scattering. *J. Phys. Chem. B* **2010**, *114*, 12948−12957.
(57) Grünberger, A.; Lai, P.-K.; Blanco, M. A.; Roberts, C. J. Coarse-grained modeling of protein second osmotic virial coefficients: sterics and short-ranged attractions. *J. Phys. Chem. B* **2013**, *117*, 763−770.
(58) Lehermayr, C.; Mahler, H.-C.; Mäder, K.; Fischer, S. Assessment of net charge and protein-protein interactions of different monoclonal antibodies. *J. Pharm. Sci.* **2011**, *100*, 2551−2562.
(59) Kumar, V.; Dixit, N.; Zhou, L. L.; Fraunhofer, W. Impact of short range hydrophobic interactions and long range electrostatic forces on the aggregation kinetics of a monoclonal antibody and a dual-variable domain immunoglobulin at low and high concentrations. *Int. J. Pharm. (Amsterdam, Neth.)* **2011**, *421*, 82−93.
(60) Fernández, C.; Minton, A. P. Effect of nonadditive repulsive intermolecular interactions on the light scattering of concentrated protein-osmolyte mixtures. *J. Phys. Chem. B* **2011**, *115*, 1289−1293.
(61) Kenrick, S.; Some, D. *Characterization of self-associating antibody solutions at high concentrations with CG-MALS*; Application Note, **2013**.
(62) Ackerson, B. J. Correlations for interacting Brownian particles. II. *J. Chem. Phys.* **1978**, *69*, 684−690.
(63) Belloni, L.; Drifford, M.; Turq, P. Non-ideality in multi-component diffusion of polyelectrolyte solutions. *J. Phys., Lett.* **1985**, *46*, 207−215.
(64) Prinsen, P.; Odijk, T. Collective diffusion coefficient of proteins with hydrodynamic, electrostatic, and adhesive interactions. *J. Chem. Phys.* **2007**, *127*, 115102.
(65) Menzen, T.; Friess, W. Temperature-ramped studies on the aggregation, unfolding, and interaction of a therapeutic monoclonal antibody. *J. Pharm. Sci.* **2014**, *103*, 445−455.
(66) Petsev, D. N.; Denkov, N. D. Diffusion of charged colloidal particles at low volume fraction: theoretical model and light scattering experiments. *J. Colloid Interface Sci.* **1992**, *149*, 329−344.
(67) Guex, N.; Peitsch, M. C. SWISS-MODEL and the Swiss-Pdb Viewer: an environment for comparative protein modeling. *Electrophoresis* **1997**, *18*, 2714−2723.
(68) Brandt, J. P.; Patapoff, T. W.; Aragon, S. R. Construction, MD simulation, and hydrodynamic validation of an all-atom model of a monoclonal IgG antibody. *Biophys. J.* **2010**, *99*, 905−913.
(69) Tang, C. L.; Alexov, E.; Pyle, A. M.; Honig, B. Calculation of pKas in RNA: on the structural origins and functional roles of protonated nucleotides. *J. Mol. Biol.* **2007**, *366*, 1475−1496.
(70) Sitkoff, D.; Sharp, K. A.; Honig, B. Accurate calculation of hydration free energies using macroscopic solvent models. *J. Phys. Chem.* **1994**, *98*, 1978−1988.
(71) Bas, D. C.; Rogers, D. M.; Jensen, J. H. Very fast prediction and rationalization of pKa values for protein-ligand complexes. *Proteins: Struct., Funct., Genet.* **2008**, *73*, 765−783.
(72) Li, H.; Robertson, A. D.; Jensen, J. H. Very fast empirical prediction and rationalization of protein pKa values. *Proteins: Struct., Funct., Genet.* **2005**, *61*, 704−721.
(73) Dolinsky, T. J.; Czodrowski, P.; Li, H.; Nielsen, J. E.; Jensen, J. H.; Klebe, G.; Baker, N. A. PDB2PQR: expanding and upgrading automated preparation of biomolecular structures for molecular simulations. *Nucleic Acids Res.* **2007**, *35*, W522−W525.
(74) Lauer, T. M.; Agrawal, N. J.; Chennamsetty, N.; Egodage, K.; Helk, B.; Trout, B. L. Developability index: a rapid in silico tool for the screening of antibody aggregation propensity. *J. Pharm. Sci.* **2012**, *101*, 102−115.
(75) Baker, N. A.; Sept, D.; Joseph, S.; Holst, M. J.; McCammon, J. A. Electrostatics of nanosystems: application to microtubules and the ribosome. *Proc. Natl. Acad. Sci. U. S. A.* **2001**, *98*, 10037−10041.
(76) *The PyMOL Molecular Graphics System*, Version 1.3r1; Schrödinger LLC: New York, 2010.
(77) Harris, L. J.; Skaletsky, E.; McPherson, A. Crystallographic structure of an intact IgG1 monoclonal antibody. *J. Mol. Biol.* **1998**, *275*, 861−872.
(78) Lošdorfer Božič, A.; Podgornik, R. Symmetry effects in electrostatic interactions between two arbitrarily charged spherical shells in the Debye-Hückel approximation. *J. Chem. Phys.* **2013**, *138*, 074902.
(79) Snyder, J. P. *Map Projections: A Working Manual*; USGS Numbered Series 1395; U.S. Department of the Interior, U.S. Geological Survey: Washington, DC, 1987
(80) Gliko, O.; Pan, W.; Katsonis, P.; Neumaier, N.; Galkin, O.; Weinkauf, S.; Vekilov, P. G. Metastable liquid clusters in super- and undersaturated protein solutions. *J. Phys. Chem. B* **2007**, *111*, 3106−3114.
(81) Collins, K. D.; Washabaugh, M. W. The Hofmeister effect and the behaviour of water at interfaces. *Q. Rev. Biophys.* **1985**, *18*, 323−422.
(82) Xie, W. J.; Gao, Y. Q. A simple theory for the Hofmeister series. *J. Phys. Chem. Lett.* **2013**, *4*, 4247−4252.
(83) Markovich, T.; Andelman, D.; Podgornik, R. Surface tension of electrolyte interfaces: ionic specificity within a field-theory approach. *J. Chem. Phys.* **2015**, *142*, 044702.
(84) Boström, M.; Parsons, D. F.; Salis, A.; Ninham, B. W.; Monduzzi, M. Possible origin of the inverse and direct hofmeister series for lysozyme at low and high salt concentrations. *Langmuir* **2011**, *27*, 9504−9511.
(85) Esfandiary, R.; Hayes, D. B.; Parupudi, A.; Casas-finet, J.; Bai, S.; Samra, H. S.; Shah, A. U.; Sathish, H. A. A systematic multitechnique approach for detection and characterization of reversible self-association during formulation development of therapeutic antibodies. *J. Pharm. Sci.* **2013**, *102*, 62−72.
(86) Blanco, M. A.; Sahin, E.; Li, Y.; Roberts, C. J. Reexamining protein-protein and protein-solvent interactions from Kirkwood-Buff analysis of light scattering in multi-component solutions. *J. Chem. Phys.* **2011**, *134*, 225103.
(87) Petsev, D. N.; Thomas, B. R.; Yau, S. T.; Vekilov, P. G. Interactions and aggregation of apoferritin molecules in solution: effects of added electrolytes. *Biophys. J.* **2000**, *78*, 2060−2069.

DOI: 10.1021/acs.jpcb.5b02459
J. Phys. Chem. B XXXX, XXX, XXX−XXX

(88) Petsev, D. N.; Vekilov, P. G. Evidence for non-DLVO hydration interactions in solutions of the protein apoferritin. *Phys. Rev. Lett.* **2000**, *84*, 1339−1342.
(89) Kern, N.; Frenkel, D. Fluid-fluid coexistence in colloidal systems with short-ranged strongly directional attraction. *J. Chem. Phys.* **2003**, *118*, 9882−9889.
(90) Zhang, Y.; Cremer, P. S. The inverse and direct Hofmeister series for lysozyme. *Proc. Natl. Acad. Sci. U. S. A.* **2009**, *106*, 15249−15253.
(91) Kurut, A.; Lund, M. Solution electrostatics beyond pH: a coarse grained approach to ion specific interactions between macromolecules. *Faraday Discuss.* **2013**, *160*, 271−278.
(92) Finet, S.; Skouri-Panet, F.; Casselyn, M.; Bonneté, F.; Tardieu, A. The Hofmeister effect as seen by SAXS in protein solutions. *Curr. Opin. Colloid Interface Sci.* **2004**, *9*, 112−116.
(93) Boström, M.; Tavares, F. W.; Finet, S.; Skouri-Panet, F.; Tardieu, A.; Ninham, B. W. Why forces between proteins follow different Hofmeister series for pH above and below pI. *Biophys. Chem.* **2005**, *117*, 217−224.
(94) Schwierz, N.; Horinek, D.; Netz, R. R. Reversed anionic hofmeister series: the interplay of surface charge and surface polarity. *Langmuir* **2010**, *26*, 7370−7379.
(95) Adžić, N.; Podgornik, R. Charge regulation in ionic solutions: thermal fluctuations and Kirkwood-Schumaker interactions. *Phys. Rev. E* **2015**, *91*, 022715.
(96) Borkovec, M.; Jönsson, B.; Koper, G. J. M. In *Surface and Colloid Science*; Matijević, E., Ed.; Surface and Colloid Science 16; Springer: New York, 2001; pp 99−339.
(97) Zhang, J. In *Protein-Protein Interactions — Computational and Experimental Tools*; Cai, W., Ed.; InTech: Rijeka, Croatia, 2012.
(98) Lund, M.; Jönsson, B. Charge regulation in biomolecular solution. *Q. Rev. Biophys.* **2013**, *46*, 265−281.
(99) Adžić, N.; Podgornik, R. Field-theoretic description of charge regulation interaction. *Eur. Phys. J. E: Soft Matter Biol. Phys.* **2014**, *37*, 5.
(100) Healy, T. W.; Chan, D.; White, L. R. Colloidal behaviour of materials with ionizable group surfaces. *Pure Appl. Chem.* **1980**, *52*, 1207−1219.
(101) Chan, D. Y. A simple algorithm for calculating electrical double layer interactions in asymmetric electrolytes−poisson-boltzmann theory. *J. Colloid Interface Sci.* **2002**, *245*, 307−310.
(102) Nap, R. J.; Božič, A. L.; Szleifer, I.; Podgornik, R. The role of solution conditions in the bacteriophage PP7 capsid charge regulation. *Biophys. J.* **2014**, *107*, 1970−1979.
(103) Bianchi, E.; Blaak, R.; Likos, C. N. Patchy colloids: state of the art and perspectives. *Phys. Chem. Chem. Phys.* **2011**, *13*, 6397.
(104) Giacometti, A.; Romano, F.; Sciortino, F. *Janus Particle Synthesis, Self-Assembly and Applications*; The Royal Society of Chemistry: Cambridge, U.K., 2012; pp 108−137.
(105) Lund, M.; Jungwirth, P. Patchy proteins, anions and the Hofmeister series. *J. Phys.: Condens. Matter* **2008**, *20*, 494218.
(106) Roberts, C. J.; Blanco, M. A. Role of anisotropic interactions for proteins and patchy nano-particles. *J. Phys. Chem. B* **2014**, *118*, 12599−12611.
(107) Bratko, D.; Striolo, A.; Wu, J. Z.; Blanch, H. W.; Prausnitz, J. M. Orientation-averaged pair potentials between dipolar proteins or colloids. *J. Phys. Chem. B* **2002**, *106*, 2714−2720.
(108) Ninham, B. W.; Yaminsky, V. Ion binding and ion specificity: the Hofmeister effect and Onsager and Lifshitz theories. *Langmuir* **1997**, *13*, 2097−2108.
(109) Kunz, W.; Boström, M. *Recent Trends in Surface and Colloid Science*; World Scientific: Singapore, 2012; Vol. *12*.

DOI: 10.1021/acs.jpcb.5b02459
J. Phys. Chem. B XXXX, XXX, XXX−XXX